Petroleum Science 23 (2026) 3576–3586

Contents lists available at ScienceDirect

Petroleum Science

journal homepage: www.keaipublishing.com/en/journals/petroleum-science

Original Paper

# Co-pyrolysis of oily sludge and lignin for fabrication of high-performance adsorbent for oily wastewater treatment

Wang-Yuan Zhang [a], Fang Xu [b], Qi Li [a,*], Yao-Zhong Zhang [c], San-Bao Dong [d,**]

[a] College of Petroleum Engineering, Xi'an Shiyou University, Xi'an, 710068, Shaanxi, China
[b] Xi'an Changqing Chemical Group Co., Ltd., Xi'an, 710065, Shaanxi, China
[c] State Key Laboratory of Water Engineering Ecology and Environment in Arid Area, Xi'an University of Technology, Xi'an, 710048, Shaanxi, China
[d] College of Chemistry and Chemical Engineering, Xi'an Shiyou University, Xi'an, 710068, Shaanxi, China

ARTICLE INFO

*Article history:*
Received 2 December 2025
Received in revised form
1 March 2026
Accepted 1 March 2026
Available online 4 March 2026

Edited by Yan-Hua Sun

*Keywords:*
Co-pyrolysis
Active material
Oily sludge
Biomass
Adsorption

ABSTRACT

Oily sludge, a hazardous by-product of the petroleum industry, poses significant environmental risks due to its elevated levels of hydrocarbons and heavy metals. As conventional disposal methods often lead to secondary pollution or inefficient resource recovery, this study investigates the synergistic pyrolysis of oily sludge with lignin to produce high-performance adsorbents for oily wastewater treatment. Thermogravimetric analyses demonstrated complementary properties and a synergistic co-pyrolysis effect between the two feedstocks. Kinetic analysis employing the Coats–Redfern method revealed that the co-pyrolysis of oily sludge and lignin significantly decreased the apparent activation energy while increasing the pre-exponential factor, confirming the lignin's catalytic role in enhancing pyrolysis efficiency. The optimal adsorbent, produced at an oily sludge-to-lignin mass ratio of 1:5, exhibited a specific surface area of 1324.5 $m^2$/g, abundant micropores, and diverse surface functional groups, as confirmed by SEM and FT-IR analyses. Under optimized conditions—an adsorbent dosage of 1.0 g/L, contact time of 40 min, and pH 7—this material effectively removed residual oil from synthetic oily wastewater and maintained over 70% removal efficiency after five regeneration cycles, highlighting its reusability. Finally, the chemical transformations of various components during the co-pyrolysis of oily sludge and biomass materials are elucidated.
© 2026 The Authors. Publishing services by Elsevier B.V. on behalf of KeAi Communications Co. Ltd. This is an open access article under the CC BY-NC-ND license (http://creativecommons.org/licenses/by-nc-nd/4.0/).

## 1. Introduction

Oily sludge is an unavoidable hazardous by-product produced during entire process of petroleum extraction, transportation, refining, storage, and utilization (Teng et al., 2021). Statistics reveal that China alone generates over 5 million tons annually, while the global volume requiring treatment surpasses 1 billion tons (Wang et al., 2018). Oily sludge exhibits a complex composition and is challenging to treat, characterized by a high oil content and considerable dewatering difficulties. As a result, it has been classified as hazardous waste in the national dangerous waste catalogue. Compared to other sludge types, oily sludge contains substantial quantities of pollutants such as polycyclic aromatic hydrocarbons and heavy metals. These contaminants can easily migrate and disperse into the atmosphere, water bodies, and soil. If improperly managed, they pose substantial risks to the environment. Due to its complex composition and high pollutant load, the effective treatment and resource utilization of oily sludge have become pressing environmental challenges (Fu et al., 2025). Biomass materials—renewable, abundant, and cost-effective—are derived from agricultural, forestry, industrial, and domestic wastes, offering significant potential for sustainable development (Hentati et al., 2022). The co-pyrolysis of widely available biomass materials with oily sludge not only addresses the disposal challenges associated with sludge but also facilitates the high-value utilization of biomass resources (Cheng et al., 2016).

Current disposal technologies for oily sludge primarily encompass incineration, landfilling, biological treatment, and chemical extraction (Zubaidy and Abouelnasr, 2010). However,

* Corresponding author.
** Corresponding author.
*E-mail addresses:* liqi@xsyu.edu.cn (Q. Li), dongsanbao@xsyu.edu.cn (S.-B. Dong).
Peer review under the responsibility of China University of Petroleum (Beijing).

https://doi.org/10.1016/j.petsci.2026.03.001
1995-8226/© 2026 The Authors. Publishing services by Elsevier B.V. on behalf of KeAi Communications Co. Ltd. This is an open access article under the CC BY-NC-ND license (http://creativecommons.org/licenses/by-nc-nd/4.0/).

these methods exhibit significant limitations, including high treatment costs and risks of secondary pollution (Gao et al., 2018). In contrast, the conversion of oily sludge into active materials through pyrolysis and carbonization can both immobilize heavy metals and reduce environmental risks, while also promoting sustainable resource utilization. The resulting active materials offer several advantages for adsorption applications, including low cost, ease of operation, renewable feedstocks, and low risk of secondary pollution. Importantly, due to the petroleum-based components in oily sludge, the derived materials show greater lipophilicity and adsorption selectivity than conventional biomass-based materials when treating oily wastewater. Active materials derived from the direct carbonization of oily sludge often suffer from limited surface area and low adsorption capacity (Niu et al., 2022). To address this limitation, co-pyrolysis of oily sludge with biomass enhances the efficiency of the pyrolysis reaction (Chen et al., 2018). This method produces composite active materials with improved structure and performance, providing a novel pathway for high-value resource recovery from oily sludge (Tang et al., 2020).

In this study, oily sludge was co-pyrolyzed with various biomass materials to prepare active material samples for the adsorption of heavy metal ions and oil components from wastewater. Thermogravimetric analysis and pyrolysis kinetic analysis were utilized to investigate the synergistic effects during the co-pyrolysis process of biomass and oily sludge. To identify suitable biomass materials and maximize the proportion of oily sludge in the co-carbonization process, the micro-porous structures of the resulting active materials were characterized through SEM and BET analyses. The adsorption performance of the active materials derived from biomass and oily sludge was systematically evaluated. Finally, the reaction process of the synergistic pyrolysis between biomass and oily sludge was analyzed in detail.

## 2. Materials and methods

### 2.1. Materials

The oily sludge sample was collected from a settling tank at Changqing Oilfield. Oligosaccharides, alkali lignin, lignin, and xylan fiber (particle size: 0–0.4 mm) were purchased from Xi'an Chemical Reagent Co., Ltd., while *n*-dodecane and sodium dodecyl sulfate (SDS, $C_{12}H_{25}SO_4Na$) (analytical reagent grade) were obtained from Tianjin Kermel Chemical Reagent Co., Ltd.

### 2.2. The preparation of adsorption material

The oily sludge and biomass materials were mixed evenly according to the mass ratios of 1:1, 1:3, and 1:5. The mixture of oily sludge and biomass materials and $K_2CO_3$ powder were evenly mixed at a mass ratio of 1:1 and then placed in a tubular furnace for pyrolysis reaction. $K_2CO_3$, KOH, and $ZnCl_2$ were selected as activators, and the yields of active materials prepared under different types of catalysts were tested. The mixture was then heated in a furnace under a nitrogen ($N_2$) atmosphere at a heating rate of 10 °C/min from room temperature to 600 °C, held for 1 h, and further heated to 800 °C at the same rate (10 °C/min) for an additional hour. After pyrolysis, the sample was allowed to cool naturally, ground into a fine powder using a ball mill (QM-3SP2, Nanjing Nanda Instrument Co., Ltd., China), and washed repeatedly with deionized water until neutrality was achieved. Finally, the product was dried at 105 °C for 4 h to obtain the active material (Hui et al., 2020).

### 2.3. Analysis of basic physical properties of raw materials

In accordance with GB/T 30732-2014 standard, the moisture content, ash content, volatile matter content, and fixed carbon content of oily sludge and four types of biomass materials were determined. The elemental composition of oily sludge and the four biomass materials (C, H, O, S, and N) was analyzed using an elemental analyzer (Vario EL/microcube, Elementar Analysensysteme GmbH, Germany). Additionally, changes in the mass of the raw materials with temperature were evaluated using a thermogravimetric analyzer (TGA/DSC 1, Mettler-Toledo, Switzerland) at temperatures ranging from 30 to 800 °C (Zhang Y. et al., 2018).

### 2.4. Characterization of active material

The pore volume distribution, pore size, and specific surface area of the active materials were analyzed using a microporous analyzer (ASAP, 2020; Micromeritics, USA), while their microstructures were examined by SEM characterization (SEM, JSM-6390A, Jeol, Japan). The functional groups and elemental composition of the active materials were characterized by Fourier transform infrared spectroscopy (Nicolet 670, Thermo Fisher, USA) and X-ray diffraction (K-Alpha, Thermo Fisher Scientific, USA), respectively (Song et al., 2010). Additionally, the residual oil content in oily wastewater was quantified by an infrared oil analyzer (GH-800, Guohuan High-Tech Automation Technology Institute, Beijing, China).

### 2.5. Preparation of oily wastewater

For the adsorption tests, oily wastewater was prepared with a water:diesel:sodium lauryl sulfate mass ratio of 99:1:0.03. The mixture was initially blended and then stirred using a variable frequency high-speed mixer at 8000 r/min for 30 min, after which it was left to stand. The upper layer of the oil film was then removed, and the lower layer of the emulsion was collected and stored in a dark-colored glass bottle.

### 2.6. Regeneration of active materials

After adsorption, the active material was placed in a pyrolysis tank and regenerated at 600 °C for 60 min under a $N_2$ atmosphere. Following regeneration, it was cooled to room temperature under an $N_2$ atmosphere.

## 3. Results and discussion

### 3.1. Physical property analysis of raw materials

The industrial and element analyses of biomass materials and oily sludge were conducted to assess the chemical composition adaptability of each raw material and to investigate the influence

**Table 1**
Proximate and elemental analyses of oily sludge and biomass materials.

| Sample | Proximate analysis, wt% | | | | Elementary analysis, wt% | | | | |
|---|---|---|---|---|---|---|---|---|---|
| | $M_{ad}$ | $A_{ad}$ | $V_{ad}$ | $FC_{ad}$ | C | H | O | N | S |
| Oily sludge | 8.4 | 61.2 | 24.5 | 5.9 | 23.2 | 6.1 | 3.7 | 0.3 | 0.9 |
| Oligosaccharide | 12.6 | 1.6 | 65.5 | 20.3 | 46.3 | 3.5 | 37.6 | 0.2 | 0.2 |
| Alkali lignin | 13.2 | 1.2 | 69.7 | 15.6 | 45.4 | 3.8 | 36.4 | 0.2 | 0.3 |
| Xylan fiber | 14.9 | 0.8 | 68.1 | 16.2 | 43.4 | 4.1 | 40.3 | 0.1 | 0.3 |
| Lignin | 15.7 | 1.0 | 71.4 | 11.8 | 48.4 | 3.6 | 38.8 | 0.2 | 0.1 |

Notes: M: water content, A: ash content, V: volatile component, FC: fixed carbon.

of individual components on the performance of activated materials. The experimental results are listed in Table 1.

The biomass materials and oily sludge samples were used for elemental and industrial evaluations. The experimental results are listed in Table 1. The industrial analysis revealed that the sludge had a high ash content of 61.2%. These findings suggest that the residual amount of oily sludge after calcination was high and the high ash content could impede the development of the internal pores of the active material (Jing et al., 2011). The elemental analysis indicated that the oily sludge possessed a relatively low oxygen concentration of only 3.7%, implying that the active material derived from the oily sludge included fewer oxygen-containing functional groups. In contrast, the proximate analysis of the four biomass materials revealed higher levels of volatile components and fixed carbon. Moreover, the elemental analysis indicated that all biomass materials contain more than 30% oxygen element, significantly higher than oily sludge. Therefore, using the co-carbonization method to prepare active material from both biomass materials and oily sludge can promote the formation of internal pores in the resulting active material (Murungi and Sulaimon, 2022). Furthermore, the higher oxygen concentration in biomass may enhance the active material's production of functional groups that include oxygen (Ma et al., 2021).

### 3.2. Thermogravimetric analysis of raw materials

The pyrolysis curves of oily sludge and four distinct types of biomass materials are illustrated in Fig. 1.

As illustrated in Fig. 1(a), the pyrolysis of oily sludge can be primarily divided into three stages. In the first stage (25–100 °C), a 6.4% weight loss occurs, primarily due to the evaporation of some light hydrocarbon and a minor quantity of external water (Wu et al., 2023). As the temperature further increases to 400 °C, a further 5.2% weight loss is observed, mainly attributed to the volatilization and pyrolysis of lighter components. Upon reaching 600 °C, the mass loss rate is 3.6%, resulting from the decomposition of residual carbonaceous materials, the condensation polymerization of macromolecular organic compounds, and the breakdown of inorganic components. During this stage, the weight loss rate remains relatively low (Chen et al., 2018). Notably, in the range of 25–100 °C, the weight loss rates for oligosaccharides, alkali lignin, xylan fibers, and lignin are 8.7%, 9.3%, 29.4%, and 55.6%, respectively. Within this interval, the biomass weight loss is primary caused by the evaporation of free or adsorbed water, along with the initial pyrolysis of unstable components (Baba Hamed et al., 2020). When temperatures exceed 500 °C, the residual biomass consists mainly of ash and highly graphitized carbon, which are chemically inert and resist further decomposition at elevated temperatures (Skubiszewska-Zięba et al., 2017).

### 3.3. Co-pyrolysis of oily sludge and biomass materials

The TG curves of oily sludge and different types of biomass materials mixed in different proportions are shown in Fig. 2.

As illustrated in Fig. 2, the TG curves display diverse patterns that vary with the ratio of oily sludge to biomass material. In all cases, the residual mass of active material from mixture decreases with increasing temperature. The initial mass loss is primarily attributed to the evaporation of lighter oil components and water from the oily sludge. Further, the final residual mass of the mixture decreases as the proportion of biomass material increases, suggesting that a larger fraction of the biomass material undergoes carbonized (Zakzeski et al., 2010). As shown in Fig. 2(d), a lignin-to-oily sludge mass ratio of 1:5 yields a solid yield of 42.1%. The combination of lignin as a carbon enhancer with oily sludge produces higher yields of active material compared to the other three biomass materials tested.

### 3.4. Selections of biomass types and proportions

The microscopic morphology of the active materials prepared by mixing the oily sludge and different biomass materials at different mass ratios are shown in Fig. 3.

Fig. 3 presents the SEM images of the active materials synthesized from oily sludge blended with various biomass materials. As illustrated in Fig. 3(a), the active material derived from oily sludge alone is predominantly composed of solid particles, exhibiting a granular morphology with no discernible pores. In contrast, Fig. 3(b–j) reveals that the active materials produced by co-pyrosis of oily sludge with biomass components possess a rough external surface and an irregular porous structure. Among them, when lignin is used as the carbonization agent, the resulting active material develops a more diverse pore structure characterized by a honeycomb-like network of channels (Hu et al., 2020). Consequently, lignin and oily sludge were selected for the preparation of

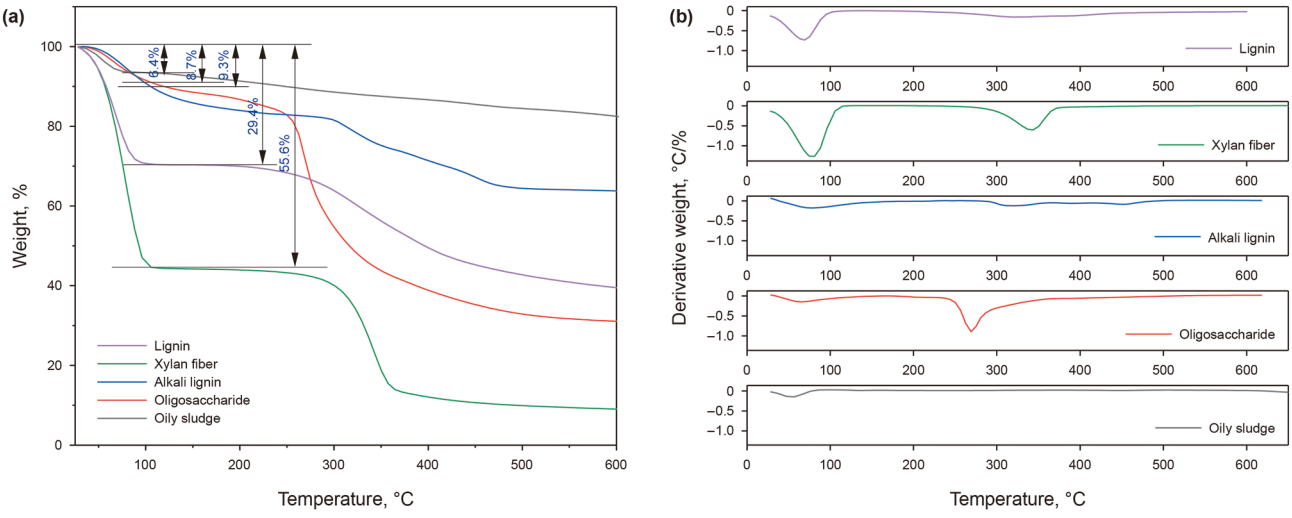


**Fig. 1.** TG curves (**a**) and DTG curves (**b**) of different materials.

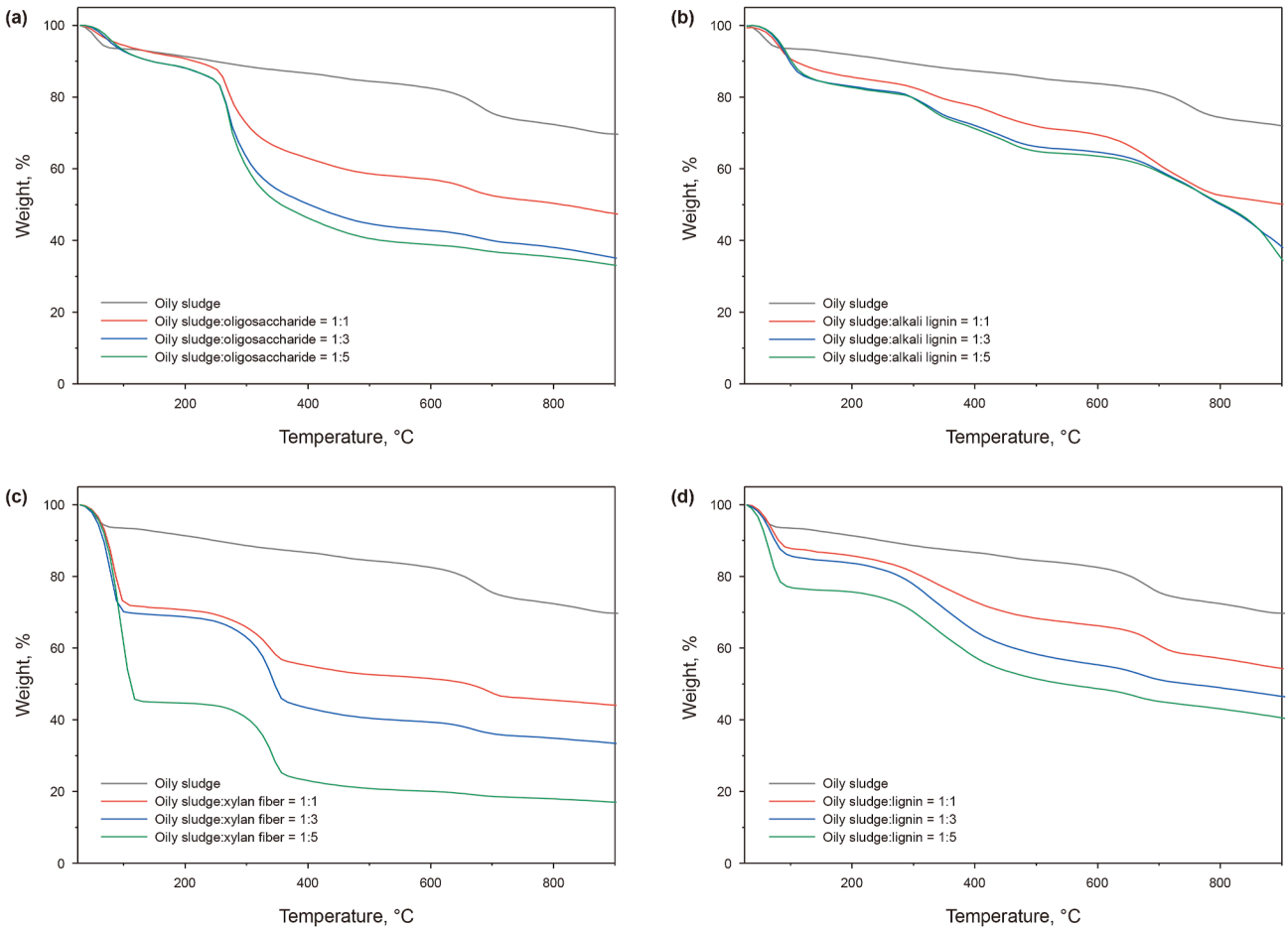


**Fig. 2.** TG curves of oily sludge mixed with oligosaccharides (**a**), alkali lignin (**b**), xylan fibers (**c**), and lignin (**d**) at different ratios.

the active material. Additional SEM characterization was conducted to determine the optimal blending ratio (Du et al., 2021).

The microscopic morphologies of the active materials prepared by mixing oily sludge with varying proportions of lignin are shown in Fig. 3(f–j). As the lignin content increased, the active material surface showed a rich pore structure. The active material particles exhibited a loose, honeycomb-like morphology and their irregular surfaces contained numerous voids and interstitial spaces, indicating a large specific surface area (Li et al., 2025). Fig. 2(d) demonstrates that the active material synthesized at a lignin-to-oily sludge mass ratio of 1:5 exhibited the most intricate surface pore structure among all tested ratios. Therefore, this ratio was selected as optimal for all subsequent experiments.

### 3.5. Screening and evaluation of activators

Different types of activators were chosen to promote the co-pyrolysis of oily sludge and lignin, and the resulting product yields were evaluated. The experimental results are presented in Table 2.

Table 2 shows that, under identical experimental conditions, the yields of the active materials prepared using $K_2CO_3$, KOH, and $ZnCl_2$ as activators were 32.6%, 29.7%, and 27.5%, respectively. Among these, $K_2CO_3$ demonstrated the most effective activation performance. As an alkaline activator, $K_2CO_3$ promotes the complete carbonization of crude oil components in oily sludge, thereby improving product yield. In addition, the decomposition of $K_2CO_3$ at elevated temperatures further strengthens the formation of pore structures within the active material. This approach optimizes pore development while maximizing the retention of the carbon skeleton, thereby achieving a favorable balance between specific surface area and product yield.

### 3.6. Kinetics analysis of co-pyrolysis of oily sludge and lignin

Oily sludge and lignin contain various complex constituents, which complicate their co-pyrolysis characterized by numerous chain reactions and parallel reactions. Developing kinetic models to characterize the pyrolysis behavior of oily sludge and lignin can better elucidate their co-pyrolysis. The co-pyrolysis of oily sludge and lignin mixtures under a programmed temperature ramp can be described by the following kinetic equation (Wang et al., 2019).

$$\frac{d\alpha}{dt} = Kf(\alpha) \tag{1}$$

$$f(\alpha) = (1-\alpha)^n \tag{2}$$

$$\alpha = \frac{m_0 - m_t}{m_0 - m_\infty} \tag{3}$$

$$k = A\exp\left(-\frac{E}{RT}\right) \tag{4}$$

where $\alpha$ is the conversion rate; $m_0$ is the initial mass; $m_\infty$ is the final residual mass; $m_t$ is the sample mass at time $t$; $f(\alpha)$ is the

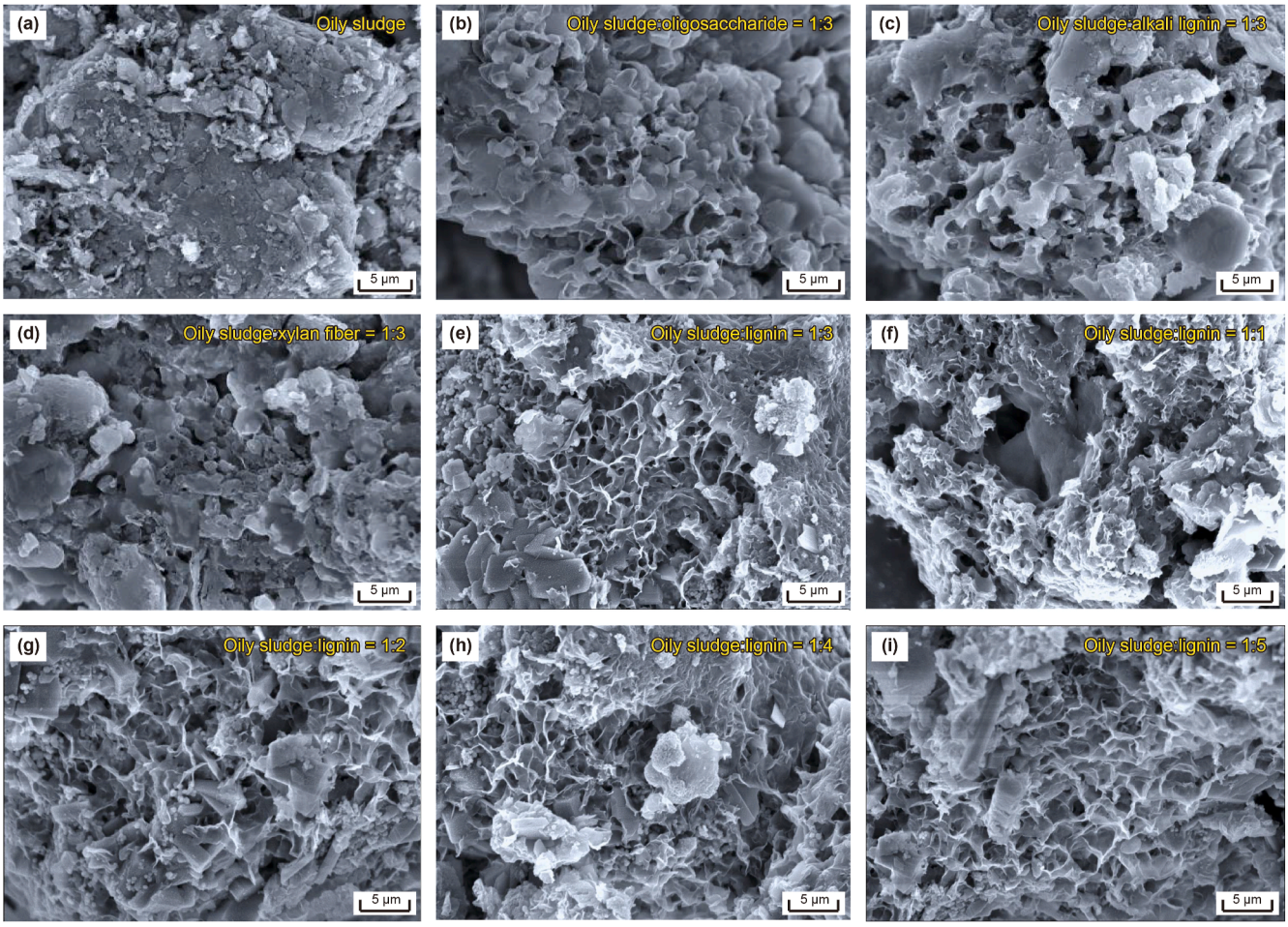


**Fig. 3.** SEM images of active materials prepared by oily sludge and biomass materials.

**Table 2**
Yields of products prepared using different activators.

| Activator | Yield, % |
|---|---|
| $K_2CO_3$ | 32.6 |
| KOH | 29.7 |
| $ZnCl_2$ | 27.5 |

pyrolysis reaction mechanism model; $n$ denotes the reaction order; $k$ is the rate constant; $E$ is the apparent activation energy, kJ/mol; $A$ is the pre-exponential factor, $min^{-1}$, $R$ is the gas constant, 8.314 J/(mol·K).

The functional form of $f(\alpha)$ depends only on the reaction type or mechanism. It is generally assumed that $f(\alpha)$ is independent of temperature and time and is a function soley of $\alpha$. By rearranging and simplifying Eqs. (1)–(4), Eq. (5) is obtained (Varsha et al., 2021).

$$\frac{d\alpha}{dt} = A(1-\alpha)^n \exp\left(-\frac{E}{RT}\right) \tag{5}$$

Substituting the pyrolysis heating rate $\beta = dT/dt$ into the above equation and simplifying gives Eq. (6).

$$\frac{d\alpha}{dT} = \frac{A}{\beta}\exp\left(-\frac{E}{RT}\right) f(\alpha) = \frac{A}{\beta}\exp\left(-\frac{E}{RT}\right)(1-\alpha)^n \tag{6}$$

By applying the Coats–Redfern integral method to the above equation, separation of variables and integration yield Eqs. (7) and (8).

$$\ln\left[\frac{-\ln(1-\alpha)}{T^2}\right] = \ln\left[\frac{AR}{\beta E}\left(1-\frac{2RT}{E}\right)\right] - \frac{E}{RT}n = 1 \tag{7}$$

$$\ln\left[\frac{-\ln(1-\alpha)^{1-n}}{T^2(1-n)}\right] = \ln\left[\frac{AR}{\beta E}\left(1-\frac{2RT}{E}\right)\right] - \frac{E}{RT}n \neq 1 \tag{8}$$

Based on literature review and computational analysis, both the pyrolysis of oily sludge and that of lignin are first-order reaction kinetics, therefore $n = 1$. In general, $2RT/E \ll 1$. Consequently, $1 - 2RT/E \approx 1$, and the term $\ln\left[\frac{AR}{\beta E}\left(1-\frac{2RT}{E}\right)\right]$ may be approximated as a constant. Simplifying the above expression yields Eq. (9) (Liu et al., 2021).

$$\ln\left[\frac{-\ln(1-\alpha)}{T^2}\right] = \ln\frac{AR}{\beta E} - \frac{E}{RT} \tag{9}$$

Therefore, $\ln\left[-\ln(1-\alpha)/T^2\right]$ exhibits a linear relationship with $1/T$. By fitting these two variables, the slope and intercept of the line can be used to determine the apparent activation energy $E$ and pre-exponential factor $A$ (Li et al., 2021). The fitted curves for the reaction stages corresponding to the pyrolysis of oily sludge and lignin, both individually and when mixed in various proportions, are shown in Fig. 4. The pyrolysis kinetic parameters derived from the Coats–Redfern model are presented in Table 3.

As illustrated in Table 3, the pre-exponential factor of lignin was significantly greater than that of oily sludge over the temperature

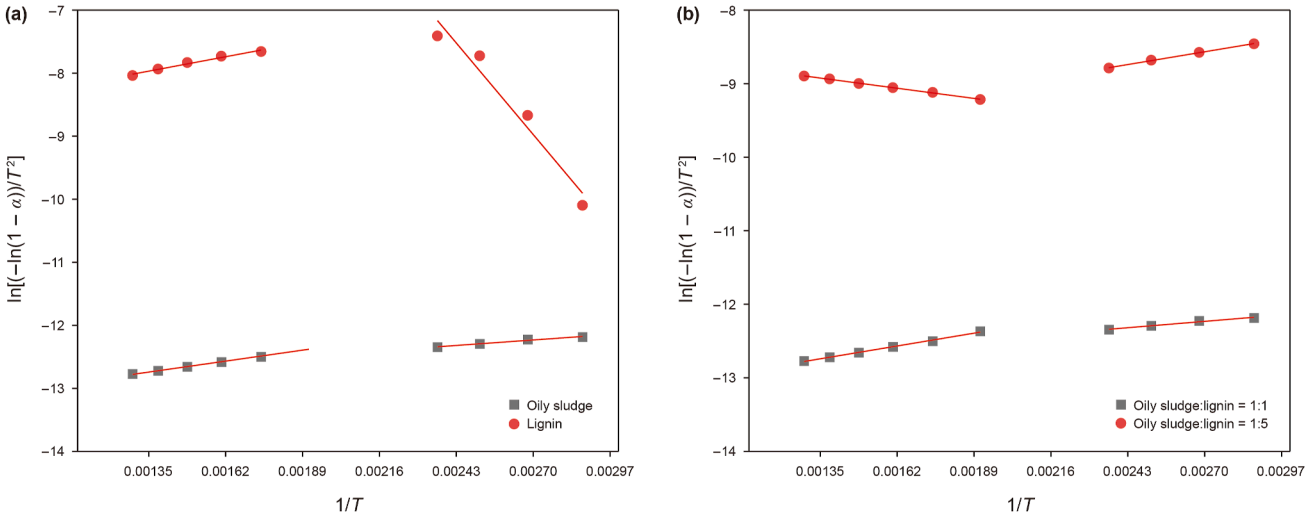


**Fig. 4.** Fitted curves for the reaction stages of oily sludge and lignin pyrolyzed separately (**a**) and co-pyrolyzed after blending at different ratios (**b**).

**Table 3**
Pyrolysis kinetic parameters for oily sludge and lignin at different ratios calculated using the Coats–Redfern model.

| Mass ratio of oily sludge to lignin | $\beta$, °C/min | Temperature range, °C | $E$, kJ/mol | $A$, min$^{-1}$ | $R^2$ |
|---|---|---|---|---|---|
| 1:0 | 10 | 25–150 | 53.58 | $7.75 \times 10^{-3}$ | 0.9955 |
| | 10 | 250–500 | 107.33 | $1.23 \times 10^{-4}$ | 0.9726 |
| 0:1 | 10 | 25–150 | 5.973 | 24.4 | 0.9719 |
| | 10 | 250–500 | 8.418 | 30.4 | 0.9336 |
| 1:1 | 10 | 25–150 | 43.97 | $9.82 \times 10^{-3}$ | 0.9954 |
| | 10 | 250–500 | 85.76 | $3.95 \times 10^{-3}$ | 0.9753 |
| 1:5 | 10 | 25–150 | 16.51 | 0.210 | 0.9847 |
| | 10 | 250–500 | 10.68 | 0.178 | 0.9965 |

ranges of 25–150 and 250–500 °C. A larger pre-exponential factor indicates a faster reaction rate, demonstrating that during independent pyrolysis, the volatilization and release rate of lignin was substantially higher than that of oily sludge, which aligns with the TGA curves. The activation energies of oily sludge were determined to be 53.58 and 107.33 kJ/mol in the ranges of 5–150 and 250–500 °C, respectively, indicating that pyrolysis of oily sludge requires greater energy absorption and exhibits relatively lower reactivity. In comparison to oily sludge, lignin exhibits lower activation energy, indicating that its thermal degradation occurs more readily with a lower energy barrier. This correlates with the substantial mass loss observed for lignin within this temperature range in the TGA curve.

When the lignin-to-oily sludge mass ratio was established at 1:1, a significant reduction in the apparent activation energy ($E$) accompanied by an increase in the pre-exponential factor ($A$) was observed. These kinetic alterations suggest that the incorporation of lignin significantly enhances the pyrolysis rate of oily sludge, thereby promoting the overall thermal decomposition. This catalytic effect became more pronounced with further increase in lignin content, strongly confirming the positive role of lignin in promoting the pyrolysis of oily sludge. Consequently, co-pyrolysis of oily sludge and lignin can improve the pyrolysis efficiency of oily sludge and enhance the quality of the three-phase products after pyrolysis of oily sludge.

### 3.7. Specific surface area and porosity analysis

The BET results of the active material prepared by co-pyrolysis of oily sludge and lignin are shown in Fig. 5 and Table 4.

As illustrated in Fig. 5(a), the $N_2$ adsorption–desorption isotherms of the active material derived from oily sludge and lignin, as well as that derived from lignin alone, display type IV behavior with an H4 hysteresis loop, indicating the presence of mesoporous structures (Zhang Z.Y. et al., 2018). $N_2$ adsorption remained low in the low-pressure region but increased significantly at relative pressures above 0.45, and the adsorption amount was larger with an obvious hysteresis loop (Hou et al., 2025). The situation pertains to the filling of micropores, which is characteristic of the typical adsorption–desorption isotherms associated with active materials containing narrow cleavage pores (Liang et al., 2025).

The specific surface area of the active material produced by mixing oily sludge and lignin was significantly higher than that of the active material derived from oily sludge alone and slightly higher than that obtained from lignin alone. This indicates that lignin plays a role in the pyrolytic charring of oily sludge. As illustrated in Fig. 5(b), lignin displays a pore distribution predominantly characterized by mesopores, accompanied by a minor proportion of micropores. In contrast, the active materials exhibit a hierarchical pore structure that is concentrated in both microporous and mesoporous ranges. This architecture offers numerous adsorption sites through micropores while utilizing mesopores as efficient transport channels, thereby improving both equilibrium capacity and adsorption kinetics.

### 3.8. XRD and FT-IR

The XRD pattern and FT-IR spectrum of the activated carbon prepared by co-pyrolysis of oily sludge and lignin with $K_2CO_3$ activation are presented in Fig. 6.

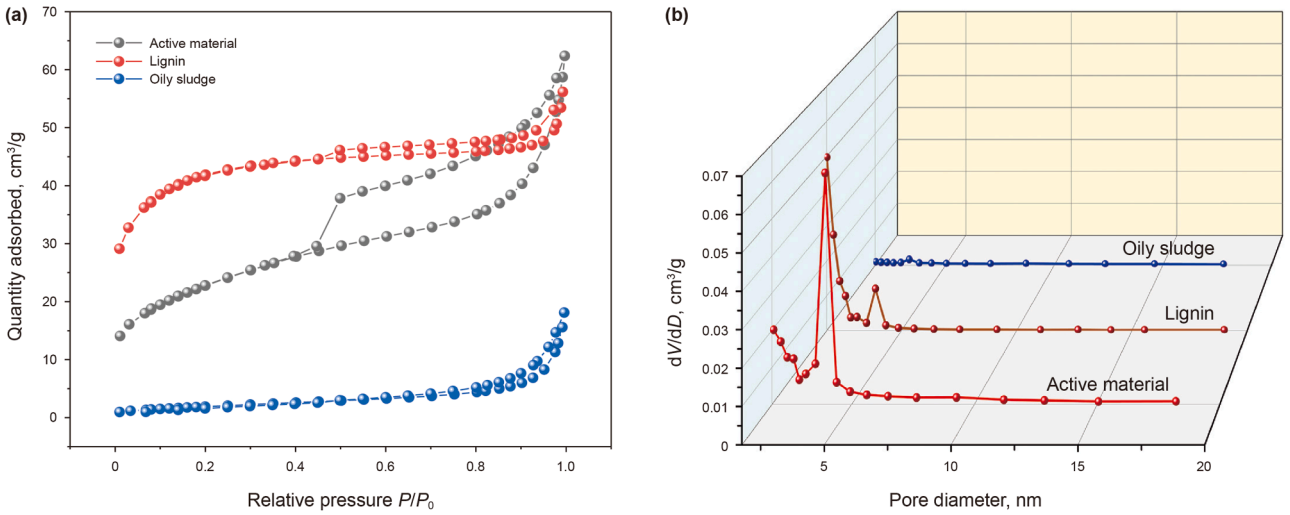


**Fig. 5.** $N_2$ adsorption–desorption isotherms (**a**) and pore size distributions (**b**) of the activated material.

**Table 4**
Specific surface area and pore structure of the active material.

| Sample | BET surface area, $m^2/g$ | Pore volume, $cm^3/g$ | Average mesopore diameter, nm |
|---|---|---|---|
| The active material | 1324.544 | 0.0869 | 3.5224 |
| Lignin | 1091.419 | 0.0765 | 4.8777 |
| Oily sludge | 54.537 | 0.0249 | 12.6394 |

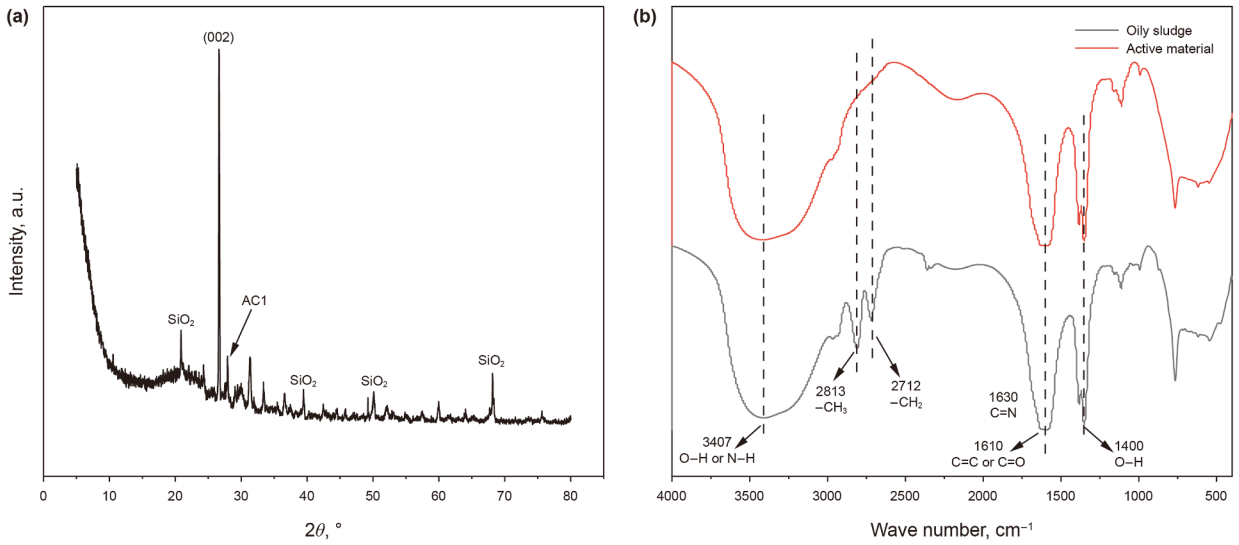


**Fig. 6.** XRD pattern (**a**) and FT-IR spectrum (**b**) of the active material derived from co-pyrolysis of oily sludge and lignin.

As illustrated in Fig. 6(a), the active material corresponds to the graphite (002) crystal plane at around 26°, exhibiting a sharp peak characteristic of AC1, low degree of disorder, and high degree of graphitization (Wu et al., 2024). Consequently, following carbonization, the raw materials consist entirely of amorphous carbon, resulting in the formation of irregular microcrystalline structures characterized by numerous pore formations. Additionally, the active material also contains $SiO_2$ and no other crystals are present (Alzahrani, 2025).

The FT-IR spectra of the active material and the oily sludge are presented in Fig. 6(b). The absorption peak at 3407 $cm^{-1}$ is attributed to the stretching vibration of O–H or N–H bonds. For the oily sludge, the peaks at 2712 and 2813 $cm^{-1}$ correspond to the C–H bond stretching vibration of $–CH_3$ and $–CH_2–$ groups, respectively (Skubiszewska-Zięba et al., 2017). After calcination, the peaks at 2712 and 2813 $cm^{-1}$ exhibited an evident decrease, indicating that most of the organic compounds in the oily sludge were decomposed at elevated temperatures.

### 3.9. Adsorption effect of active material on oily wastewater

The removal of oily wastewater by the active materials prepared with oily sludge and lignin in different ratios are shown in Fig. 7.

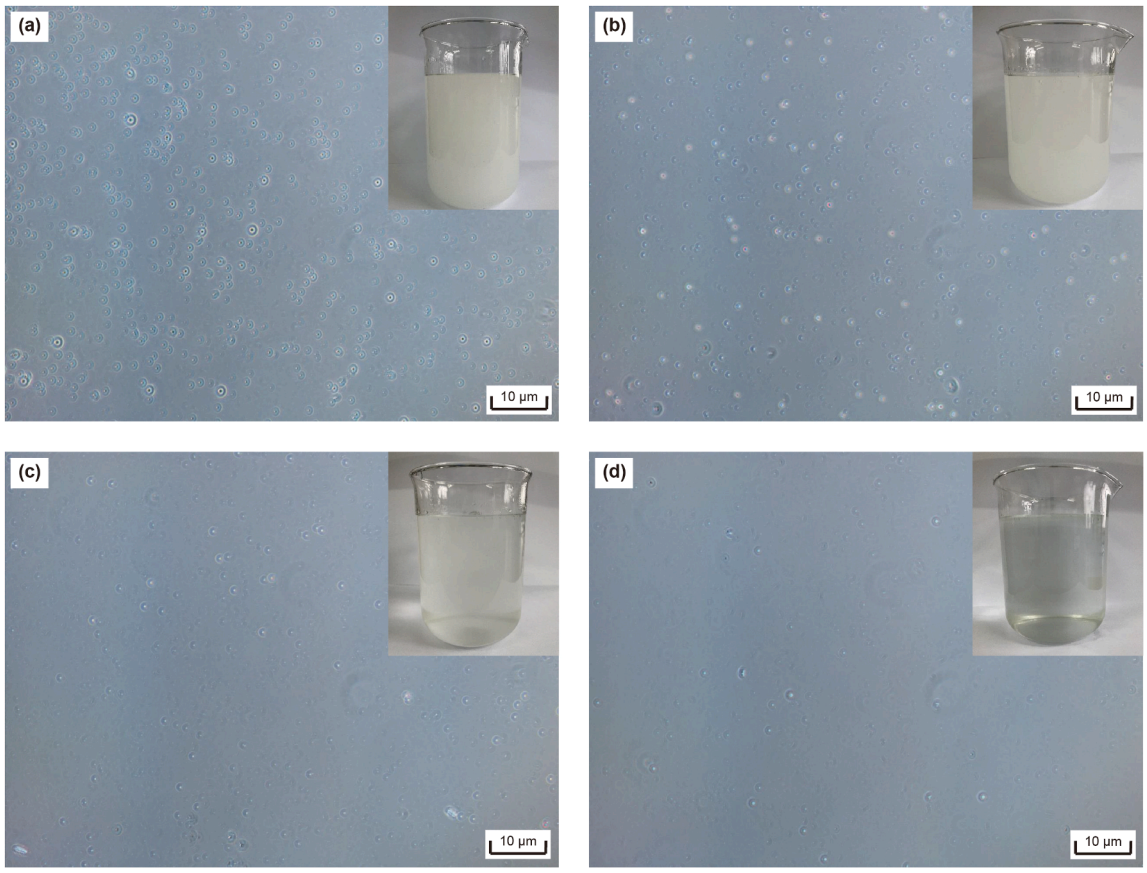


**Fig. 7.** Effects of active materials prepared by oily sludge and lignin at different ratios on oily wastewater treatment: (**a**) blank, (**b**) 1:1, (**c**) 1:3, (**d**) 1:5.

As illustrated in Fig. 7, the control group lacking active materials demonstrated significantly higher turbidity, with water-in-oil (O/W) emulsion droplets clearly visible under microscopic observation. Progressive improvement in emulsion clarification was observed as the mass ratio of oily sludge to lignin increased from 1:1 to 1:5. The active material prepared from oily sludge and lignin at a 1:5 ratio exhibited the most effective emulsification and adsorption performance for oily wastewater. The adsorption effect of active material may be greatly enhanced using lignin as a carburization agent. The high oil absorption efficiency of the active material can be attributed to its large specific surface area and abundant internal pores and voids (Huang et al., 2022).

### 3.10. Effect of conditions on the adsorption of oily wastewater by active material

The adsorption performance of the active materials under different conditions was tested and the experimental results are shown in Fig. 8.

The effect of active material concentration on the adsorption of residual oil in oily wastewater is illustrated in Fig. 8(a). The adsorption capacity of the active material for residual oil increased progressively with the dosage of the active substance. A higher concentration of active material provides more active sites in the solution, thereby enhancing the overall adsorption capacity (Huang et al., 2022). When the concentration of the active substance was increased to 1.0 g/L, the residual oil concentration in the solution decreased sharply from 1152.37 to 230.35 mg/L. However, when the concentration of the active substance exceeded 1.0 g/L, there was no significant change in the residual oil concentration in the solution.

The effect of adsorption time on the adsorption performance of the active material is illustrated in Fig. 8(b). At a constant dosage, the adsorption of residual oil by the active material increased progressively with longer adsorption time. When the adsorption time exceeded 40 min, the adsorption capacity of the active material no longer changed significantly. At the beginning of the adsorption, a great number of adsorption sites are available on the active material, resulting in a higher adsorption rate (Li and Wei, 2016). As adsorption proceeds, the number of effective adsorption sites decreases, leading to a gradual decrease in the availability of oil molecules and a corresponding reduction in the adsorption rate (Hui et al., 2020).

The effect of solution pH on the adsorption performance of the active material is illustrated in Fig. 8(c). As the pH of the solution increased from 5 to 9, the concentration of residual oil first decreased and then increased. The active material exhibited optimal adsorption performance at pH = 7, with the oil concentration reduced to 229.58 mg/L. Under neutral conditions, the emulsification tendency of oil droplets is inhibited, preventing their dispersion into charged, stable droplets and thereby facilitating adsorption (Monteiro et al., 2025). In addition, the various functional groups present in the active material remain chemically stable in a neutral environment, and the integrity of its porous structure is well maintained (Yalcinkaya et al., 2017).

The reusability of the active material was assessed through cyclic adsorption–regeneration tests. As illustrated in Fig. 8(d), the oil removal efficiency gradually decreased with an increasing number of regeneration cycles, yet remained above 70% after five

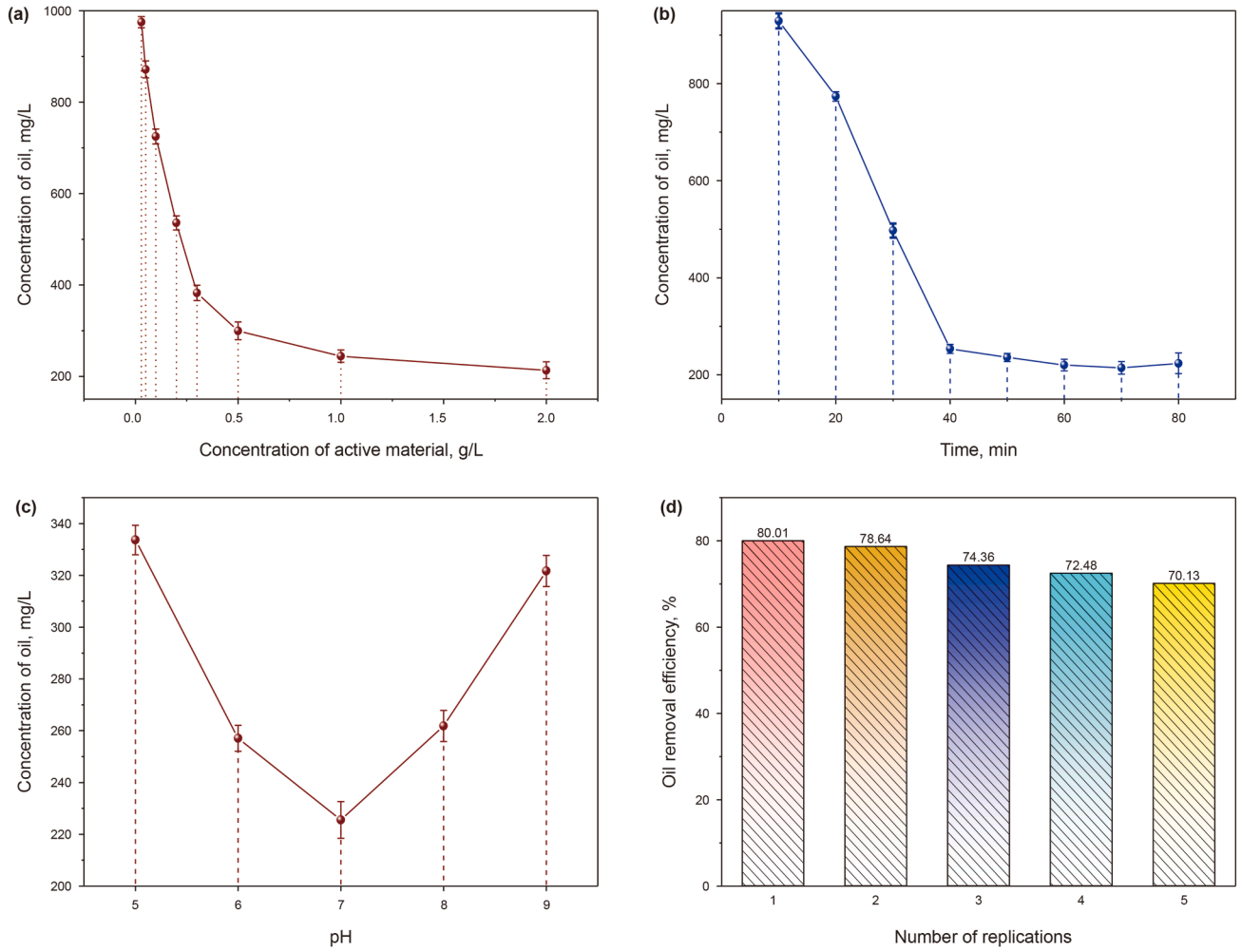


**Fig. 8.** Effect of concentration (**a**), time (**b**), pH (**c**), and number of replications (**d**) on the adsorption performance of active material.

consecutive runs. These findings demonstrate the material's promising regeneration potential and practical recyclability (Medeiros et al., 2022). During high-temperature regeneration, partial collapse or blockage occurs within the microporous structure of the active material, and surface oxygen-containing functional groups diminish due to thermal decomposition. This leads to in a reduction in specific surface area and weakened adsorption capacity. Simultaneously, refractory heavy crude oil components, heavy metal ions, and inorganic ash gradually accumulate within the pores of the active material, occupying and masking effective adsorption sites.

### 3.11. Comparison of similar product

A comparison of the novel active material with similar adsorbents is presented in Table 5.

As presented in Table 5, the high-performance active material derived from two types of industrial waste—oily sludge and lignin—exhibits an impressive specific surface area of 1325 $m^2/g$. This significantly outperforms commercial standard activated carbon (921 $m^2/g$), silica gel (467 $m^2/g$), and activated alumina (335 $m^2/g$). The active material employs oily sludge and lignin as raw materials. Through a co-pyrolysis process, it not only enhances the mesoporous structure and specific surface area but also achieves zero-cost substitution of raw materials, thereby demonstrating substantial competitiveness in both economic and technological dimensions.

### 3.12. Pyrolysis process between oily sludge and lignin

Through an analysis of the fundamental physical properties of oily sludge and lignin, as well as the characterization of the

**Table 5**
Performance comparison of the active material with similar adsorbent materials.

| Type | Specific surface area, $m^2/g$ | Average mesopore diameter, nm |
|---|---|---|
| Active material | 1325 | 3.52 |
| Standard activated carbon | 921 | 3.48 |
| Silicone | 467 | 4.15 |
| Activated alumina | 335 | 4.74 |

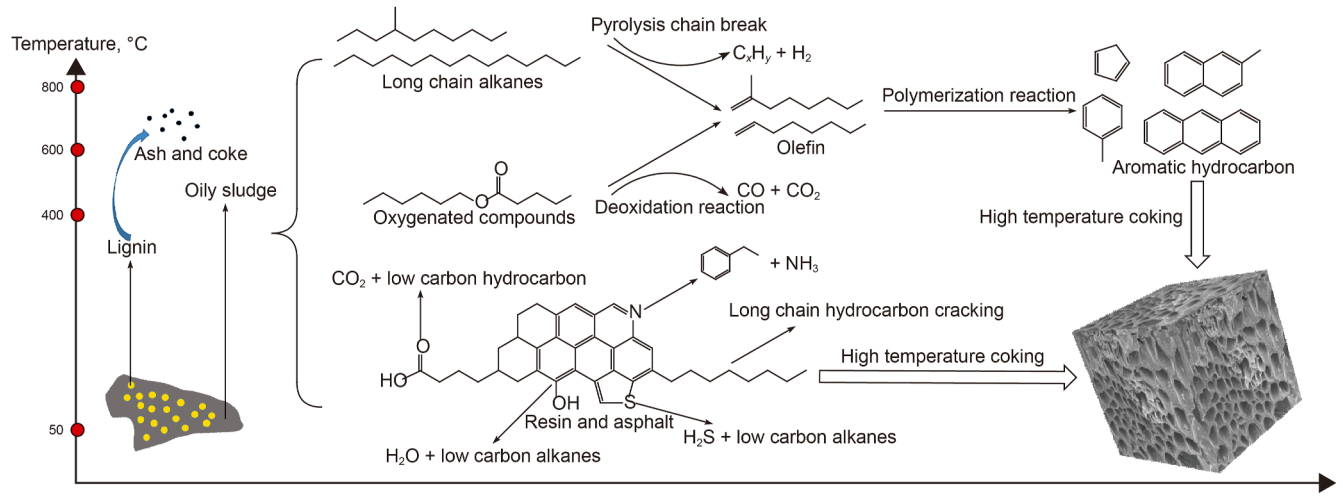


**Fig. 9.** The pathway and mechanism of synergistic pyrolysis between oily sludge and lignin.

functional groups and microstructure of the active materials prepared by their synergistic pyrolysis, further speculation was made on the chemical reactions that transpired during the high-temperature pyrolysis of oily sludge and lignin. The results are presented in Fig. 9.

As depicted in Fig. 9, lignin, due to its relatively low activation energy, undergoes pyrolysis prior to the components of oily sludge, converting into biochar at temperatures below 400 °C. Subsequently, the heavy constituents in the oily sludge come into contact with the biochar and adsorb onto its surface, leading to an increased yield of pyrolysis residue. The long-chain alkanes present in the oily sludge first experience thermal cracking and dehydrogenation, generating olefins and releasing hydrogen gas. Concurrently, oxygen-containing compounds also produce olefins via decarbonylation and decarboxylation reactions, resulting in the release of CO and $CO_2$. At elevated temperatures, these olefins further undergo dehydrogenation polymerization, yielding mono and polycyclic aromatic hydrocarbons. Under sustained high-temperature conditions, these aromatic hydrocarbons, along with resin and asphaltene fractions, become carbonized and adhere to the inorganic surfaces within the oily sludge, ultimately producing a highly porous active material with exceptional adsorption performance.

## 4. Conclusions

In this study, an active material with high adsorption efficiency for oily wastewater was synthesized from oily sludge by leveraging the pyrolysis-promoting effect of biomass materials. Among four types of biomass materials evaluated, lignin exhibited the most favorable synergistic effect with oily sludge. This synergy was confirmed through chemical experiments and thermal decomposition kinetics analysis. The active material prepared by co-pyrolysis of oily sludge at a mass ratio of 1:5 exhibited the largest specific surface area (1324.5 $m^2/g$) and the strongest adsorption capacity for the emulsion. SEM and RT-IR analyses revealed that the active material possesses abundant microporous structures and a diverse type of surface functional groups. For oily wastewater with an initial oil concentration of 1152.37 mg/L, the optimal adsorption conditions were determined as follows: adsorbent dosage of 1.0 g/L, contact time of 40 min, and pH = 7. After five reuse cycles, the active material retained an oil removal rate of 70.13%, demonstrating excellent recyclability. This study presents a new method of resource utilization of oily sludge and offers new insights into the green treatment and resource recovery of oily sludge.

## CRediT authorship contribution statement

**Wang-Yuan Zhang:** Writing – original draft, Investigation, Data curation, Conceptualization. **Fang Xu:** Validation, Formal analysis, Data curation. **Qi Li:** Methodology, Formal analysis, Conceptualization. **Yao-Zhong Zhang:** Investigation, Funding acquisition, Formal analysis. **San-Bao Dong:** Writing – review & editing, Methodology, Investigation, Funding acquisition.

## Declaration of competing interest

The authors declare that they have no known competing financial interests or personal relationships that could have appeared to influence the work reported in this paper.

## Acknowledgements

This work was financially supported by the Open Research Fund Program of the State Key Laboratory of Eco-hydraulics in Northwest Arid Region, Xi'an University of Technology (Grant No. 2020KFKT-8), the Natural Science Foundation of China (No. 52204046), the Natural Science Foundation of Shaanxi Province, China (No. 2025 JC-YBMS-573), and the Youth Innovation Team Research Program Project of Educational Commission of Shaanxi Province (No. 23JP103).

## References

Alzahrani, N., 2025. Co-pyrolysis of waste plastics and tires: Influence of interaction on product oil and gas composition. J. Energy Inst. 118, 101908. https://doi.org/10.1016/j.joei.2024.101908.

Baba, H.S., 2020. Optimizing the transport of cuttings with ecological drilling muds: Application to directional well. J. Braz. Soc. Mech. Sci. Eng. 42 (12), 619. https://doi.org/10.1007/s40430-020-02698-4.

Chen, B., Zhao, L., Duan, M., et al., 2018. The chemical degradation of the oil sludge produced from polymer flooding in offshore oilfield. Energy Sci. Eng. 6 (5), 484–489. https://doi.org/10.1002/ese3.222.

Chen, G., Yuan, W., Yan, J., et al., 2018. Zn(II) complex catalyzed coupling aquathermolysis of water-heavy oil-methanol at low temperature. Pet. Chem. 58 (3), 197–202. https://doi.org/10.1134/s0965544118030039.

Cheng, S., Takahashi, F., Gao, N., et al., 2016. Evaluation of oil sludge ash as a solid heat carrier in the pyrolysis process of oil sludge for oil production. Energy Fuels. 30 (7), 5970–5979. https://doi.org/10.1021/acs.energyfuels.6b00648.

Du, M., Li, J., Wang, F., et al., 2021. The sludge-based adsorbent from oily sludge and sawdust: Preparation and optimization. Environ. Technol. 42 (20), 3164–3177. https://doi.org/10.1080/09593330.2020.1725138.
Fu, Q., Liao, X., Zhong, W., et al., 2025. Combined chemical-biological method for efficient clean treatment of oily sludge. Water, Air, Soil Pollut. 236 (2), 124. https://doi.org/10.1007/s11270-025-07767-9.
Gao, Y.X., Ding, R., Chen, X., et al., 2018. Ultrasonic washing for oily sludge treatment in pilot scale. Ultrasonics 90 (17), 1–4. https://doi.org/10.1016/j.ultras.2018.05.013.
Hentati, D., Abed, R., Abotalib, N., 2022. Biotreatment of oily sludge by a bacterial consortium: Effect of bioprocess conditions on biodegradation efficiency and bacterial community structure. Front. Microbiol. 13, 998076. https://doi.org/10.3389/fmicb.2022.998076.
Hou, C.P., Wang, Q., Liu, Q., et al., 2025. Review: Development and application of porous materials to antibiotic drug adsorption and removal. J. Water Proc. Eng. 69, 106583. https://doi.org/10.3389/fmicb.2022.998076.
Hu, S., Wang, H., Wang, F., et al., 2020. Synthesis of kappa fiber modified graphite carbon nitride with outstanding photocatalytic phenol degradation ability. Diam. Relat. Mater. 105, 107817. https://doi.org/10.1016/j.diamond.2020.107817.
Huang, H., Li, X., Zhao, C., et al., 2022. Superhydrophobic and magnetic PS/$Fe_3O_4$ sponge for remote oil removal under magnetic driven, continuous oil collection, and oil/water emulsion separation. J. Mater. Sci. 57 (1), 336–350. https://doi.org/10.1007/s10853-021-06568-9.
Hui, K., Tang, J., Lu, H., et al., 2020. Status and prospect of oil recovery from oily sludge: A review. Arab. J. Chem. 13 (8), 6523–6543. https://doi.org/10.1016/j.arabjc.2020.06.009.
Jing, G., Luan, M., Chen, T., 2011. Prospects for development of oily sludge treatment. Chem. Technol. Fuels Oils 47 (4), 312–326. https://doi.org/10.1007/s10553-011-0301-4.
Li, B., Wei, W., 2016. Effect of lignin on the co-pyrolysis of sludge and cellulose. Energy Sources, Part A Recovery, Util. Environ. Eff. 38 (12), 1825–1831. https://doi.org/10.1080/15567036.2014.964816.
Li, D., Lei, S., Rajput, G., et al., 2021. Study on the co-pyrolysis of waste tires and plastics. Energy 226, 120381. https://doi.org/10.1016/j.energy.2021.120381.
Li, X., Liu, M., Wen, L., et al., 2025. Synergism between activated carbon and fenton reaction for organic pollutant degradation: The hitherto overlooked role of dynamic single-atom sites. Environ. Sci. Technol. 59 (26), 1283–1294. https://doi.org/10.1021/acs.est.5c01201.
Liang, Y., Zhang, Z., Wang, E., et al., 2025. Preparation of silane-free porous structure hyperelastic phosphorylated chitosan sponge reinforced with bamboo activated carbon and its efficient PM2.5 removal. Carbohydr. Polym. 352, 123237. https://doi.org/10.1016/j.carbpol.2025.123237.
Liu, J., Yang, X., Liu, H., et al., 2021. Mixed biochar obtained by the co-pyrolysis of shrimp shell with corn straw: Co-pyrolysis characteristics and its adsorption capability. Chemosphere 282, 131116. https://doi.org/10.1016/j.chemosphere.2021.131116.
Ma, Y., Yao, M., Liu, L., et al., 2021. Mechanism and characteristics of oil recovery from oily sludge by sodium lignosulfonate treatment. ACS Omega 6 (39), 25819–25827. https://doi.org/10.1021/acsomega.1c04369.
Medeiros, A., Silva, J.C., Amorim, J., 2022. Oily wastewater treatment: Methods, challenges, and trends. Processes 10 (4), 743. https://doi.org/10.3390/pr10040743.
Monteiro, K.A., Mounteer, A.H., Moreira, R.P.L., et al., 2025. Promoting a circular economy: Wastewater toxicity removal using activated carbon produced from industrial sludge. J. Environ. Chem. Eng. 13 (4), 117450. https://doi.org/10.1016/j.jece.2025.117450.
Murungi, P.I., Sulaimon, A.A., 2022. Petroleum sludge treatment and disposal techniques: A review. Environ. Sci. Pollut. Control Ser. 29 (27), 40358–40372. https://doi.org/10.1007/s11356-022-19614-z.
Niu, A., Sun, X., Lin, C., 2022. Trend in research on characterization, environmental impacts and treatment of oily sludge: A systematic review. Molecules 27 (22), 7795. https://doi.org/10.3390/molecules27227795.
Skubiszewska, Z.J., Charmas, B., Kołtowski, M., 2017. Active carbons from waste biochars. J. Therm. Anal. Calorim. 130 (1), 15–24. https://doi.org/10.1007/s10973-017-6143-5.
Song, W., Liu, J., Nie, Y., 2010. Pyrolysis behaviors of oil sludge based on TG/FTIR and PY-GC/MS. Front. Environ. Sci. Eng. 4 (1), 59–64. https://doi.org/10.1007/s11783-009-0152-y.
Tang, C., Guan, J., Xie, S., 2020. Study on reutilization of pyrolytic residues of oily sludge. Int. J. Anal. Chem. 2020, 1–7. https://doi.org/10.1155/2020/8858022.
Teng, Q., Zhang, D., Yang, C., 2021. A review of the application of different treatment processes for oily sludge. Environ. Sci. Pollut. Control Ser. 28 (1), 121–132. https://doi.org/10.1007/s11356-020-11176-2.
Varsha, S.S.V., Vuppaladadiyam, A.K., Shehzad, F., et al., 2021. Co-pyrolysis of microalgae and municipal solid waste: A thermogravimetric study to discern synergy during co-pyrolysis process. J. Energy Inst. 94, 29–38. https://doi.org/10.1016/j.joei.2020.10.010.
Wang, S., Cao, B., Feng, Y., et al., 2019. Co-pyrolysis and catalytic co-pyrolysis of Enteromorpha clathrata and rice husk: Toward high-quality products. J. Therm. Anal. Calorim. 135 (4), 2613–2623. https://doi.org/10.1007/s10973-018-7334-4.
Wang, Z., Gong, Z., Wang, Z., et al., 2018. A TG-MS study on the coupled pyrolysis and combustion of oil sludge. Thermochim. Acta 663, 137–144. https://doi.org/10.1016/j.tca.2018.03.019.
Wu, L., Qi, S., Zhang, T., et al., 2024. One-step carbonization/activation synthesis of chitosan-based porous sheet-like carbon and studies of adsorptive removal for Rhodamine B. Carbohydr. Polym. 330, 121832. https://doi.org/10.1016/j.carbpol.2024.121832.
Wu, Y., You, F., Hou, S., et al., 2023. Study of a novel cross linked graft copolymer starch in water-based drilling fluid. Mater. Res. Express 10 (5), 055501. https://doi.org/10.1088/2053-1591/acd227.
Yalcinkaya, F., Siekierka, A., Bryjak, M., 2017. Preparation of fouling-resistant nanofibrous composite membranes for separation of oily wastewater. Polymers 9 (12), 679–692. https://doi.org/10.3390/polym9120679.
Zakzeski, J., Bruijnincx, P.C.A., Jongerius, A.L., et al., 2010. The catalytic valorization of lignin for the production of renewable chemicals. Chem. Rev. 110 (6), 3552–3599. https://doi.org/10.1021/cr900354u.
Zhang, Y., Kong, W., Wang, C., et al., 2018. Switching wormlike micelles of selenium-containing surfactant using redox reaction. Soft Matter 11 (38), 7469–7473. https://doi.org/10.1021/acs.langmuir.7b03837.
Zhang, Z.Y., Li, L.H., Zhang, J.S., et al., 2018. Solidification of oily sludge. Pet. Sci. Technol. 36 (4), 273–279. https://doi.org/10.1080/10916466.2017.1419482.
Zubaidy, E.A.H., Abouelnasr, D.M., 2010. Fuel recovery from waste oily sludge using solvent extraction. Process Saf. Environ. Prot. 88 (5), 318–326. https://doi.org/10.1016/j.psep.2010.04.001.